

# Twelve massless flavors and three colors below the conformal window

Zoltán Fodor<sup>a,e</sup>, Kieran Holland<sup>b</sup>, Julius Kuti<sup>\*,c</sup>, Dániel Nógrádi<sup>e</sup>, Chris Schroeder<sup>d</sup>

<sup>a</sup>Department of Physics, University of Wuppertal, Gausstrasse 20, D-42119, Germany

Jülich Supercomputing Center, Forschungszentrum, Jülich, D-52425 Jülich, Germany

<sup>b</sup>Department of Physics, University of the Pacific, 3601 Pacific Ave, Stockton CA 95211, USA

<sup>c</sup>Department of Physics 0319, University of California, San Diego, 9500 Gilman Drive, La Jolla, CA 92093, USA

<sup>d</sup>Department of Physics, University of Wuppertal, Gausstrasse 20, D-42119, Germany

<sup>e</sup>Institute for Theoretical Physics, Eötvös University, H-1117 Budapest, Hungary

## Abstract

We report new results for a frequently discussed gauge theory with twelve fermion flavors in the fundamental representation of the SU(3) color gauge group. The model, controversial with respect to its conformality, is important in non-perturbative studies searching for a viable composite Higgs mechanism Beyond the Standard Model (BSM). To resolve the controversy, we subject the model to opposite hypotheses inside and outside of the conformal window. In the first hypothesis we test chiral symmetry breaking ( $\chi$ SB) with its Goldstone spectrum,  $F_\pi$ , the  $\chi$ SB condensate, and several composite hadron states as the fermion mass is varied in a limited range with our best effort to control finite volume effects and extrapolation to the massless chiral limit. Supporting results for  $\chi$ SB from the running coupling based on the force between static sources and some preliminary evidence for the finite temperature transition are also presented. In the second test for the alternate hypothesis we probe conformal behavior driven by a single anomalous mass dimension under the assumption of unbroken chiral symmetry. Our results show a very low level of confidence in the conformal scenario. Staggered lattice fermions with stout-suppressed taste breaking are used throughout the simulations.

**Key words:** lattice simulations, electroweak sector, technicolor, conformal

## 1. Introduction

New physics at the Large Hadron Collider could be discovered in the form of some new strongly-interacting gauge theory with a composite Higgs mechanism, an idea which was outside experimental reach when it was first introduced as an attractive BSM scenario [1–9]. The original framework has been expanded by new explorations of the multi-dimensional theory space of nearly conformal gauge theories [10–17] where systematic non-perturbative lattice studies play a very important role. New experimental results at the Tevatron [18], boldly interpreted as Technicolor [19], will further stimulate lattice efforts to provide a well-controlled theoretical framework. Interesting models require the theory to be very close to, but below, the conformal window, with a running coupling which is almost constant over a large energy range. The non-perturbative knowledge of the critical flavor  $N_f^{crit}$  separating the two phases is essential and this has generated much interest and many new lattice studies [20–44].

We report new studies of an important and frequently discussed gauge theory with twelve fermion flavors in the fundamental representation of the SU(3) color gauge group. With  $N_f = 12$  being close to the critical flavor number, the model has attracted a great deal of attention in the lattice community

and off-lattice as well. To establish the chiral properties of a gauge theory close to the conformal window is notoriously difficult. If the chiral symmetry is broken, the fundamental parameter  $F$  of the chiral Lagrangian has to be small in lattice units  $a$  to control cut-off effects. Since the chiral expansion has terms with powers of  $N_f M_\pi^2 / 16\pi^2 F^2$ , reaching the chiral regime with a large number of fermion flavors is particularly difficult. The range of  $aM_\pi$  values where leading chiral logs can be identified unambiguously will require simulations in very large volumes which are not in the scope of this study. We will make a case in this report that qualitatively different expectations inside and outside the conformal window allow tests of the two mutually exclusive hypotheses without reaching down to the chiral logs at very small pion masses.

Below the conformal window, chiral symmetry is broken at zero fermion mass with a gap in the composite hadron spectrum except for the associated massless Goldstone multiplet. The analytic form of the chiral Lagrangian as a function of the fermion mass can be used to detect chiral log corrections, or to differentiate from conformal exponents in the transitional region before the chiral logs are reached at low enough Goldstone pion masses. Approximations to gauge theories with  $\chi$ SB, like their effective Nambu-Jona-Lasinio description in the large N limit, are consistent with this analysis. In sharp contrast, the spectrum inside the conformal window is gapless in all channels in the chiral limit and the scale dependence of physical quantities, like the fermion mass dependence of composite operators and

\*Corresponding author

Email address: jkuti@ucsd.edu (Julius Kuti)

their correlators, is governed by the single critical exponent  $\gamma$ .

The two competing hypotheses can be tested in search for chiral properties of gauge theories. There is a fundamental difference between the two hypotheses as implied by their respective spectra.  $\chi$ SB creates a fundamental scale  $F$  in the theory separated from the composite hadron scale with its residual baryon gap in the chiral limit. The pion mass can be varied from the  $\chi$ SB scale  $F$  to the hadron scale with a transition from the chiral log regime to a regime without chiral analysis. The conformal phase has no intrinsic scale. With  $\chi$ SB this is expected to lead to fermion mass dependence of the spectrum in the chiral log regime, or above it, quite different from the conformal behavior which is very tightly constrained near the chiral limit of the spectrum with a single critical exponent  $\gamma$  in the absence of any intrinsic scale. In a regime where lattice cutoff effects are negligible, this difference should be sufficient for tests whether the chiral loop expansion is reached, or not, on the low scale  $F$ .

In Sections 2 and 3 we present new results for the gauge model with twelve fermions in the fundamental representation. A new kind of gauge dynamics is expected to appear at intermediate distances with walking gauge coupling or a conformal fixed point. This has remained controversial with recent efforts from five lattice groups [20–30]. We have made considerable progress to resolve the controversies including tests of the chiral condensate and the spectrum which favor chiral symmetry breaking with unusual chiral dynamics. Applying the  $\chi$ SB hypothesis to the Goldstone pion,  $F_\pi$ , the chiral condensate, and the stable nucleon state collectively leads to a result of  $\chi^2/\text{dof} = 1.22$  representing a high level of confidence. With the conformal hypothesis we find  $\chi^2/\text{dof} = 8.79$  representing a very low level of confidence. Applying a global analysis to all states we measured, the contrasting behavior is somewhat less dramatic but remains significant. New results on the running coupling from the static force and our simulation of a rapid finite temperature transition in Polyakov loop distributions, reported elsewhere and expected in association with  $\chi$ SB and its restoration, provide further support for our findings. In Section 4 we will briefly summarize our conclusions with outlook for future work.

We have used the tree-level Symanzik-improved gauge action for all simulations in this paper. The conventional  $\beta = 6/g^2$  lattice gauge coupling is defined as the overall factor in front of the well-known terms of the Symanzik lattice action. Its value is  $\beta = 2.2$  for all simulations reported here for the  $N_f = 12$  model. The link variables in the staggered fermion matrix were exponentially smeared with two stout steps [53]; the precise definition of the action is given in [54]. The RHMC and HMC algorithms were deployed in all runs. For the molecular dynamics we made use of multiple time scales [55] and the Omelyan integrator [56]. Our error analysis of hadron masses which combines systematic and statistical effects follows the frequentist histogram approach of the Budapest-Marseille-Wuppertal collaboration [57]. The topological charge was monitored in the simulations with frequent changes observed.

## 2. Tests of the $\chi$ SB hypothesis

The chiral Lagrangian for the Goldstone spectrum separated from the massive composite scale of hadrons exhibits, order by order, the well-known analytic form of powers in the fermion mass  $m$  with non-analytic chiral log corrections generated from pion loops close enough to the chiral limit [58]. The exact functions  $F_\pi(m)$  and  $M_\pi(m)$  will be approximated by an analytic form in powers of  $m$  which is expected to hold over a limited  $m$  range when the Goldstone pion is in transition from the chiral log regime toward the composite hadron scale. Although this procedure has some inherent uncertainty without the chiral logs directly reached in simulations, its sharp contrast with the non-analytic fermion mass dependence of the conformal hypothesis, governed by the single exponent  $\gamma$ , is sufficient to differentiate the two hypotheses.

First, we will illustrate the fitting procedure with results on the Goldstone spectrum,  $F_\pi$ , and the chiral condensate. This will be extended to the nucleon and some other composite hadron channels to probe parity degeneracy and residual masses in the chiral limit.

### 2.1. Goldstone spectrum and $F_\pi$ from $\chi$ SB

Figure 1 shows the Goldstone pion and  $F_\pi$  as a function of the fermion mass  $m$  in the range where we can reach the infinite volume limit with confidence. The power functions of the fitting procedure in  $m$  contain the analytic contributions of the fourth order chiral Lagrangian to  $M_\pi$  and  $F_\pi$ . Although we could fit the pion spectrum with the logarithmic term included, its significance remains unclear. The rapid variation of  $F_\pi$  with  $m$  clearly shows that we would need a dense set of data in the  $m = 0.003 - 0.01$  range to reach chiral logs at this gauge coupling. This requires lattice volumes well beyond the largest size  $48^3 \times 96$  which we could deploy in our simulations.

Efforts were made for extrapolations to the infinite volume limit. At the lowest three  $m$  values, for finite volume corrections to  $M_\pi$  and  $F_\pi$ , and for all other states, we used the form

$$M_\pi(L_s, \eta) = M_\pi \left[ 1 + \frac{1}{2N_f} \frac{M^2}{16\pi^2 F^2} \cdot \widetilde{g}_1(\lambda, \eta) \right], \quad (1)$$

$$F_\pi(L_s, \eta) = F_\pi \left[ 1 - \frac{N_f}{2} \frac{M^2}{16\pi^2 F^2} \cdot \widetilde{g}_1(\lambda, \eta) \right], \quad (2)$$

where  $\widetilde{g}_1(\lambda, \eta)$  describes the finite volume corrections with  $\lambda = M_\pi \cdot L_s$  and aspect ratio  $\eta = L_t/L_s$  from the lightest pion wrapping around the lattice and coupled to the measured state [59]. The form of  $\widetilde{g}_1(\lambda, \eta)$  is a complicated infinite sum which contains Bessel functions and requires numerical evaluation. Since we are not in the chiral log regime, the prefactor of the  $\widetilde{g}_1(\lambda, \eta)$  function was replaced by a fitted coefficient. The leading term of the function  $\widetilde{g}_1(\lambda, \eta)$  is a special exponential Bessel function  $K_1(\lambda)$  which dominates in the simulation range. The fitting procedure could be viewed as the approximate leading treatment of the pion which wraps around the finite volume, whether in chiral perturbation theory, or in Lüscher's non-perturbative finite volume analysis [60] which does not require the chiral limit as long as the pion is the lightest state dominating the corrections.

Table 1: Measured masses and  $F_\pi$  with the three largest volumes in the  $m = 0.01 - 0.02$  range and the largest volume for  $m > 0.02$ . Asterisks indicate  $L_s = 32$  when different from the spatial volume of the second column.  $M_{pnuc}$  is the mass of the nucleon's parity partner.

mass	lattice	$M_\pi$	$F_\pi$	$M_{15}$	$M_{sc}$	$M_{ij}$	$M_{nuc}$	$M_{pnuc}$	$M_{Higgs}$	$M_{rho}$	$M_{A1}$
0.0100	$48^3 \times 96$	0.1647(23)	0.02474(49)	0.1650(13)	0.16437(95)	0.1657(10)	0.3066(69)	0.3051(81)	0.247(13)	0.1992(28)	0.2569(83)
0.0100	$40^3 \times 80$	0.1819(28)	0.02382(39)	0.1842(29)	0.1835(35)	0.1844(44)	0.3553(93)	0.352(16)	0.2143(81)	0.2166(73)	0.237(12)
0.0100	$32^3 \times 64$	0.2195(35)	0.02234(46)	0.2171(31)	0.194(10)	0.195(11)	0.386(16)	0.387(22)	0.2162(53)	0.239(19)	0.246(21)
0.0150	$48^3 \times 96$	0.2140(14)	0.03153(51)	0.2167(16)	0.2165(17)	0.2185(18)	0.3902(67)	0.3881(84)	0.296(13)	0.2506(33)	0.3245(87)
0.0150	$40^3 \times 80$	0.2200(23)	0.03167(53)	0.2210(21)	0.2218(30)	0.2239(34)	0.4095(84)	0.411(10)	0.291(11)	0.2574(36)	0.327(14)
0.0150	$32^3 \times 64$	0.2322(34)	0.03168(64)	0.2319(11)	0.2318(17)	0.2341(16)	0.4387(60)	0.4333(84)	0.2847(33)	0.2699(41)	0.324(16)
0.0200	$40^3 \times 80$	0.2615(17)	0.03934(56)	0.2736(22)*	0.2651(8)	0.2766(42)*	0.4673(62)	0.4699(66)	0.330(17)	0.3049(28)	0.361(32)
0.0250	$32^3 \times 64$	0.3098(18)	0.04762(53)	0.3179(17)	0.3183(18)	0.3231(20)	0.563(12)	0.563(14)	0.4137(88)	0.3683(19)	0.469(14)
0.0275	$24^3 \times 48$	0.3348(29)	0.05218(85)	0.3430(18)	0.3425(25)	0.3471(26)	0.609(21)	0.628(23)	0.460(16)	0.4050(69)	0.523(34)
0.0300	$24^3 \times 48$	0.3576(15)	0.0561(11)	0.3578(15)*	0.3726(29)	0.3790(40)	0.640(12)*	0.633(16)*	0.470(15)	0.4160(26)*	0.5222(90)*
0.0325	$24^3 \times 48$	0.3699(66)	0.0588(15)	0.3790(34)	0.3814(62)	0.3879(62)	0.680(18)	0.686(26)	0.500(21)	0.4481(39)	0.548(31)
0.0350	$24^3 \times 48$	0.3927(17)	0.06422(57)	0.4065(18)	0.4074(19)	0.4149(26)	0.703(28)	0.741(20)	0.538(30)	0.4725(64)	0.669(65)

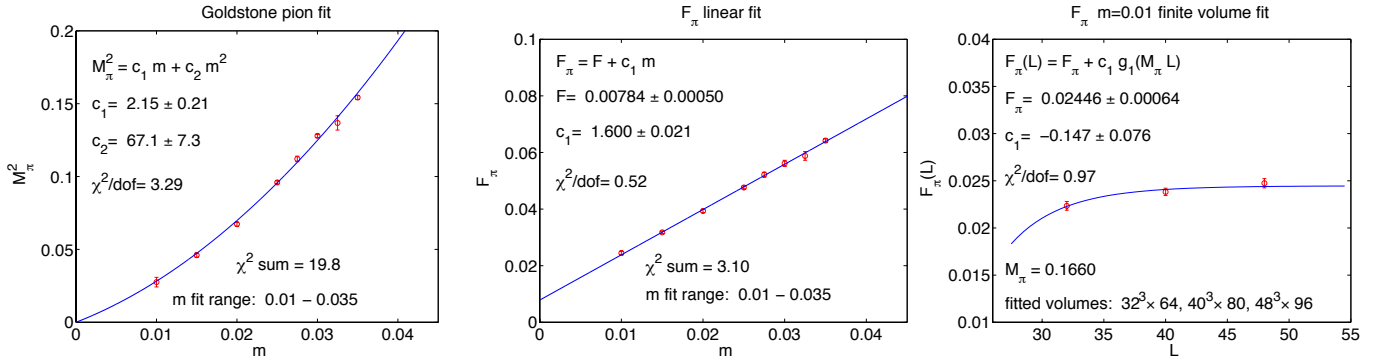


Figure 1: The Goldstone pion and  $F_\pi$  from chiral symmetry breaking are shown with the fitting procedure described in the text. A representative finite volume fit is also shown. The infinite volume limit of  $M_\pi$  was used in fits to  $F_\pi$  and other composite hadron states, like the nucleon.

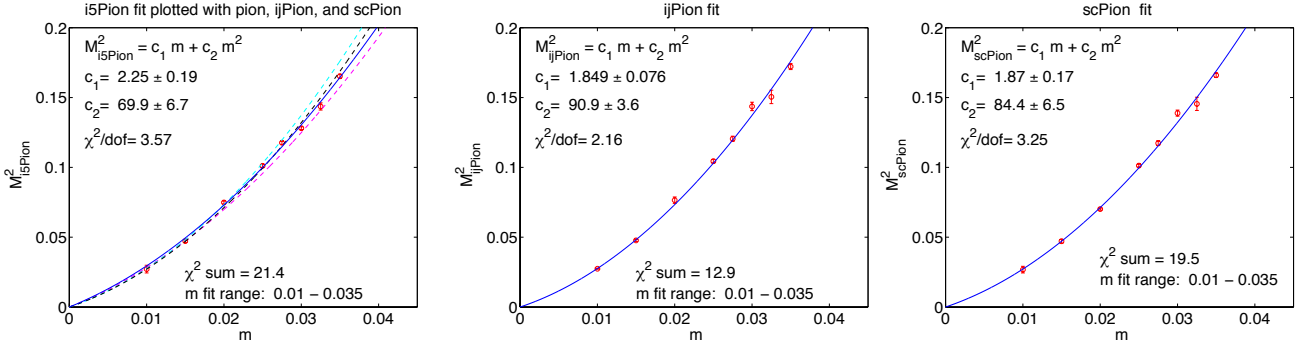


Figure 2: The non-Goldstone pion spectrum is shown. The composite left plot displays the i5Pion data and fit together with fits to the Goldstone pion (magenta), i5Pion (solid blue), scPion (black), and ijPion (cyan).

The  $M_\pi L_s > 4$  lore for volume independence is clearly not applicable in the model. We need  $M_\pi L_s > 8$  to reach volume independence. The infinite volume limits of  $M_\pi$  and  $F_\pi$  for each  $m$  were determined self-consistently from the fitting procedure using Eqs. (1,2) based on a set of  $L_s$  values with representative fit results shown in Figures 1 and 4. In the higher  $m$  range finite volume effects were hard to detect and even for the lowest  $m$  values sometimes volume dependence was not detectable for the largest lattice sizes.

Non-Goldstone pion spectra, quite different from those found in QCD, are shown in Figure 2 using standard notation. They are not used in our global analysis. The three states we designate as i5Pion, ijPion and scPion do not show any noticeable

taste breaking or residual mass in the  $m \rightarrow 0$  chiral limit. The scPion is degenerate with the i5Pion and both are somewhat split from the true Goldstone pion. The ijPion state is further split as expected but the overall taste breaking is very small across the four pion states. This is a fairly strong indication that the coupling constant  $\beta = 2.2$  where all runs are performed is close to the continuum limit. A very small residual mass at  $m = 0$  is not excluded for some non-Goldstone pion states depending on the details of the fitting procedure.

The staggered meson and baryon states and correlators we use are defined in [61]. For example, what we call the scPion and the  $f_0$  meson are identified in correlator I of Table 1 in [61]. Similarly, the i5Pion is from correlator VII, the ijPion is from

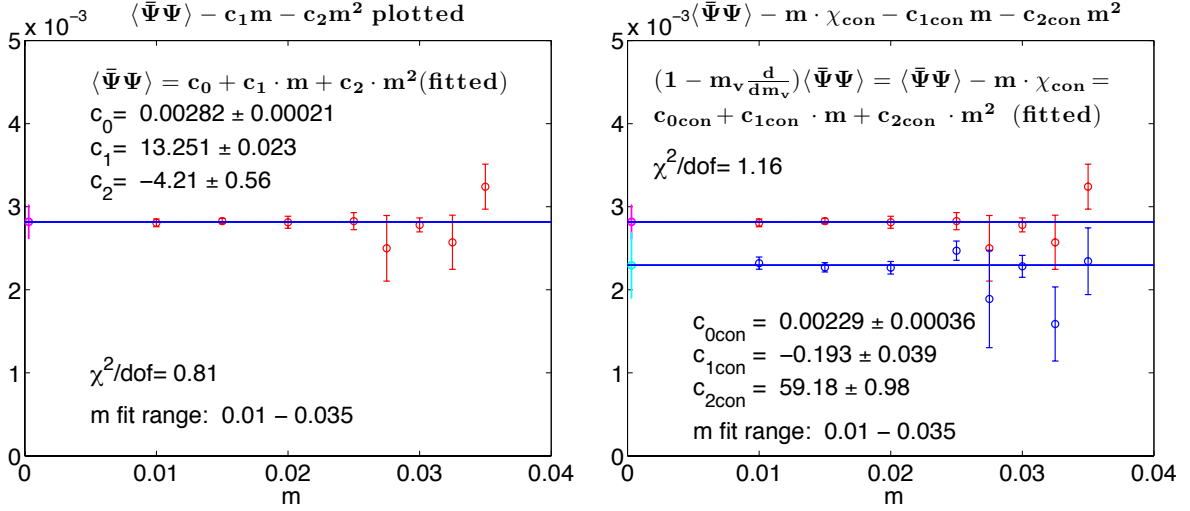


Figure 3: The chiral condensate is shown on the left. After the coefficients of the quadratic fitting function were determined, the plot shows data for  $\langle \bar{\psi} \psi \rangle - c_1 m + c_2 m^2$  for better visual display of the chiral limit at  $m = 0$  and its error (in magenta) coming from the fitted  $c_0$  constant part. The right side is the quadratic fit to  $\langle \bar{\psi} \psi \rangle - m \cdot \chi_{con}$  which is defined in the text and directly measured from zero momentum sum rules and independently from functions of the inverse staggered fermion matrix. The fitting function is  $c_{0con} + c_{1con} m + c_{2con} m^2$ . After the coefficients of the quadratic fitting function were determined, the plot shows data (blue points) for  $\langle \bar{\psi} \psi \rangle - m \cdot \chi_{con} - c_{1con} m - c_{2con} m^2$  for better visual display of the chiral limit at  $m = 0$  and its error (in cyan) coming from the fitted  $c_{0con}$  constant part. For comparison, the left side plot is redisplayed showing consistency between the two different and independent determinations of the chiral condensate in the chiral limit. For any given  $m$  always the largest volume chiral condensate data is used since the finite volume analysis is not complete. We will continue extended systematics at the lowest two or three  $m$  values which play an important role in the analysis.

correlator VIII, the rho and A1 mesons are from correlator III of Table 1. We measure the Goldstone pion in two different ways, with one of them defined in correlator II of Table 1 in the reference. The nucleon state and its parity partner are defined in correlator I of Table 2 in [61].

## 2.2. Chiral condensate

The chiral condensate  $\langle \bar{\psi} \psi \rangle$  summed over all flavors has the spectral representation [62]

$$\begin{aligned} \langle \bar{\psi} \psi \rangle &= -2m \cdot \int_0^\mu \frac{d\lambda \rho(\lambda)}{m^2 + \lambda^2} \\ &= -2m^5 \cdot \int_\mu^\infty \frac{d\lambda}{\lambda^4} \frac{\rho(\lambda)}{m^2 + \lambda^2} + c_1 \cdot m + c_3 \cdot m^3 \end{aligned} \quad (3)$$

where the UV-divergent integral is written in a twice-subtracted form in the second line [63]. The UV contribution, which is divergent when the cutoff  $a^{-1}$  is removed, has a linear term  $\approx a^{-2} \cdot m$  and there is a third-order term  $\approx m^3$  which is hard to detect for small  $m$  and survives even in the free theory limit. The IR finite contributions to the chiral Lagrangian have a constant term  $\approx BF^2$ , a linear term  $\approx B^2 \cdot m$ , a quadratic term  $\approx B^3 F^{-2} \cdot m^2$ , and higher order terms in addition to logarithmic corrections generated from chiral loops [64].

We kept a constant IR term, the linear term with UV and IR contributions, and the quadratic IR term in our fitting procedure of  $\langle \bar{\psi} \psi \rangle$ . The quadratic fit in Figure 3 gives a small non-vanishing condensate in the chiral limit which is roughly consistent with the GMOR [65] relation  $\langle \bar{\psi} \psi \rangle = 12F^2 B$  with the measured low value of  $F$  and O(1) value for  $B$  which correspond to the Goldstone pion fits in Figure 1. The deficit between the two sides of the GMOR relation is sensitive to the

fitting procedure and the uncertain determination of  $B$ . The quadratic term in the fit is a relatively small contribution and trying to identify chiral logs is beyond the scope of our simulation range.

For an independent determination, we also studied the subtracted chiral condensate operator defined with the help of the connected part  $\chi_{con}$  of the chiral susceptibility  $\chi$ ,

$$(1 - m_v \frac{d}{dm_v}) \langle \bar{\psi} \psi \rangle |_{m_v=m} = \langle \bar{\psi} \psi \rangle - m \cdot \chi_{con}, \quad (4)$$

$$\chi = \frac{d}{dm} \langle \bar{\psi} \psi \rangle = \chi_{con} + \chi_{disc},$$

$$\chi_{con} = \frac{d}{dm_v} \langle \bar{\psi} \psi \rangle_{pq} |_{m_v=m}.$$

The derivatives  $d/dm$  and  $d/dm_v$  are taken at fixed gauge coupling  $\beta$ . The derivative  $d/dm_v$  is defined in the partially quenched functional integral of  $\langle \bar{\psi} \psi \rangle_{pq}$  with respect to the valence mass  $m_v$  and the limit  $m_v = m$  is taken after differentiation. The removal of the derivative term significantly reduces the dominant linear part of the  $\langle \bar{\psi} \psi \rangle$  condensate. We find it reassuring that the two independent determinations give consistent non-vanishing results in the chiral limit as clearly shown in Figure 3.

It should be noted that the  $M_\pi$  values in the fitting range of  $m$  in our analysis are below the fitting range of previous  $N_f = 12$  work on the chiral condensate work with considerably more uncertainty from using the higher range [26]. In all fits we were on a fine-grained lattice in the pion mass range  $aM_\pi = 0.16 - 0.39$  and rho mass range  $M_\rho = 0.2 - 0.47$ . In contrast, the previous study [26] which reported conformal behavior was in the  $aM_\pi = 0.35 - 0.67$  range and rho mass range  $M_\rho = 0.39 - 0.77$ . Although our new results should be made even more definitive

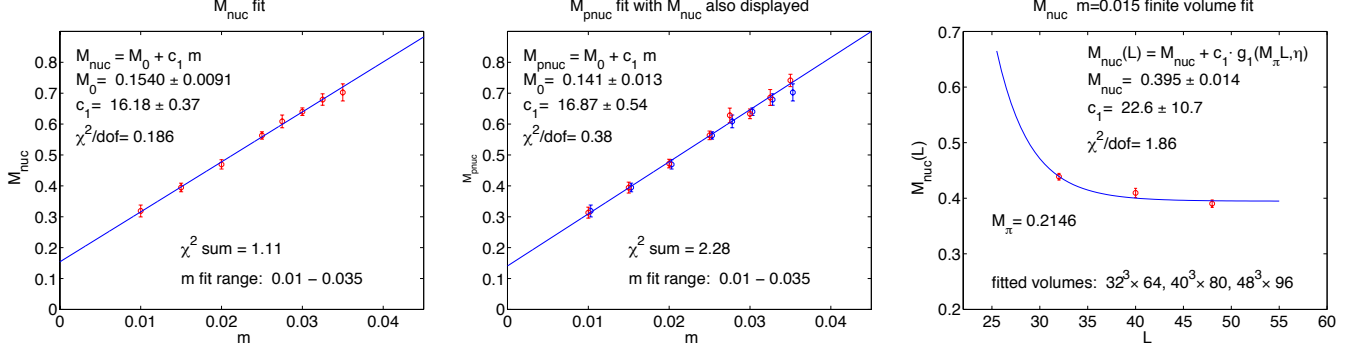


Figure 4: Nucleon and its parity partner are fitted to the constant plus linear form which are the leading contributions of the chiral Lagrangian. The blue points in the middle plot are the replotted nucleon data from the left to show the degeneracy of the two states. The plot on the right shows a representative finite volume fit.

Table 2: The chiral condensate  $\langle\bar{\psi}\psi\rangle$  and  $\langle\bar{\psi}\psi\rangle - m \cdot \chi_{con}$ , defined in the text and directly measured from zero momentum sum rules and independently from functions of the inverse staggered fermion matrix, are tabulated and used in the fits of Figure 3.

mass	lattice	$\langle\bar{\psi}\psi\rangle$	$\langle\bar{\psi}\psi\rangle - m \cdot \chi_{con}$
0.0100	$48^3 \times 96$	0.134896(47)	0.006305(73)
0.0150	$48^3 \times 96$	0.200647(31)	0.012685(56)
0.0200	$40^3 \times 80$	0.266151(72)	0.022069(76)
0.0250	$32^3 \times 64$	0.33147(10)	0.03462(12)
0.0275	$24^3 \times 48$	0.36372(40)	0.04133(59)
0.0300	$32^3 \times 32$	0.396526(84)	0.04974(13)
0.0325	$24^3 \times 48$	0.42879(33)	0.05781(45)
0.0350	$24^3 \times 48$	0.46187(27)	0.06807(40)

with higher accuracy and better control on the systematics, the evidence is quite suggestive for a small non-vanishing chiral condensate in the chiral limit.

### 2.3. Composite hadron spectrum in the chiral limit

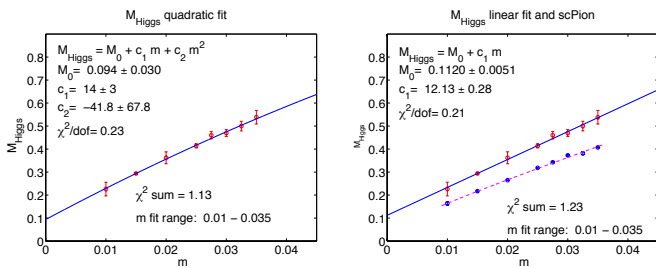


Figure 5: The Higgs ( $f_0$ ) state and its splitting from the scPion state are shown. The linear fit on the right works well for the Higgs ( $f_0$ ) state with little change when a quadratic term is included on the left. The blue scPion data points on the right and the dashed magenta fit show the fit to the scPion state. The Higgs will become a resonance in the chiral limit, the missing disconnected part also contributing, so that Higgs predictions will be challenging in future work.

It is important to investigate the chiral limit of other composite hadron states. They further test the mass splittings between physical states as the fermion mass  $m$  is varied and the measured hadron masses are subjected to chiral analysis in the  $m \rightarrow 0$  limit for important residual mass gaps above the vacuum after infinite volume extrapolation. Hadron masses also

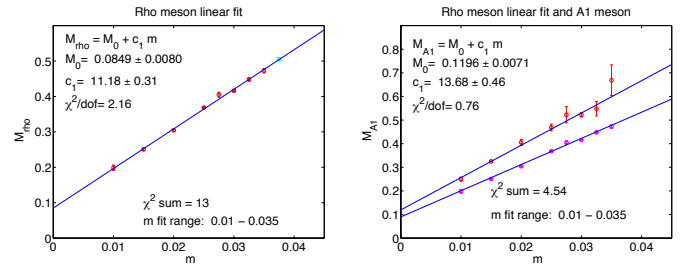


Figure 6: Rho meson and its splitting from the A1 meson are shown. On the right side the magenta points reproduce the data of the rho meson from the left together with its linear fit. The fit parameters on the right show the linear fit to the A1 meson.

provide useful information on parity splits in several channels. One composite state of great interest is the Higgs particle, if there is a chiral condensate close to the conformal window. We will briefly review new results on the nucleon state with its parity partner, the isospin partner of the Higgs ( $f_0$ ) state, and the  $\rho - A_1$  splitting.

The fermion mass dependence of the nucleon and its parity partner is shown in Figure 4 with finite volume analysis at one selected fermion mass  $m = 0.015$ . The same finite volume fit is applied as described earlier for the pion state. The leading chiral linear term in the fermion mass  $m$  extrapolates to a non-vanishing chiral limit. The parity partner is practically degenerate but this is not a surprise. Already with four flavors a near degeneracy was reported before by the Columbia group [66].

Figure 5 shows the fermion mass dependence of the Higgs particle without including the disconnected part of the relevant correlator. Strictly speaking, therefore, the state is the  $f_0$  meson with non-zero isospin. Disconnected contributions in the correlator might shift the Higgs mass, an important issue left for future clarifications. Both the linear and the quadratic fits are shown together with the non-Goldstone scPion which is split down from the Higgs ( $f_0$ ) state. The two states would be degenerate in the chiral limit with unbroken symmetry. The Higgs ( $f_0$ ) state extrapolates to a nonvanishing mass in the chiral limit with an  $M_{H(f_0)}/F$  ratio between 10 and 15.

Finally, Figure 6 shows the  $\rho$ -meson and its  $A_1$  parity partner. Both states extrapolate to non-vanishing mass in the chiral limit.

Table 3:  $V(R)$  tabulated at fermion masses  $m = 0.010$  and  $m = 0.015$  for lattice volume  $48^3 \times 96$ , and at  $m = 0.020$  for lattice volume  $40^3 \times 80$ .

$m \backslash R$	4	5	6	7	8	9	10	11	12	13	14
0.010	0.20005(49)	0.22686(84)	0.24638(12)	0.26000(28)	0.27059(55)	0.27957(82)	0.2872(10)	0.2933(21)	0.2979(42)	0.30771(31)	0.31250(82)
0.015	0.20439(21)	0.23332(35)	0.25270(39)	0.26737(85)	0.2789(17)	0.2892(28)	0.30214(36)	0.3129(11)	0.3220(31)	0.3289(12)	0.33576(43)
0.020	0.20819(39)	0.2372(16)	0.25961(99)	0.27727(55)	0.29132(74)	0.3040(11)	0.31718(24)	0.32862(31)	0.33973(78)	0.34921(77)	0.3543(55)
$m \backslash R$	15	16	17	18	19	20	21	22	23	24	
0.010	0.31755(43)	0.32186(78)	0.3263(19)	0.3308(23)	0.3339(40)	0.3364(47)	0.3417(27)	0.3453(29)	0.3466(62)	0.3554(25)	
0.015	0.34295(46)	0.35050(37)	0.35863(78)	0.36506(45)	0.36928(69)	0.3708(31)	0.3741(55)	0.3817(59)	0.3897(71)		
0.020	0.3625(58)	0.3768(24)	0.3939(107)	0.3946(10)	0.4026(13)	0.4085(30)					

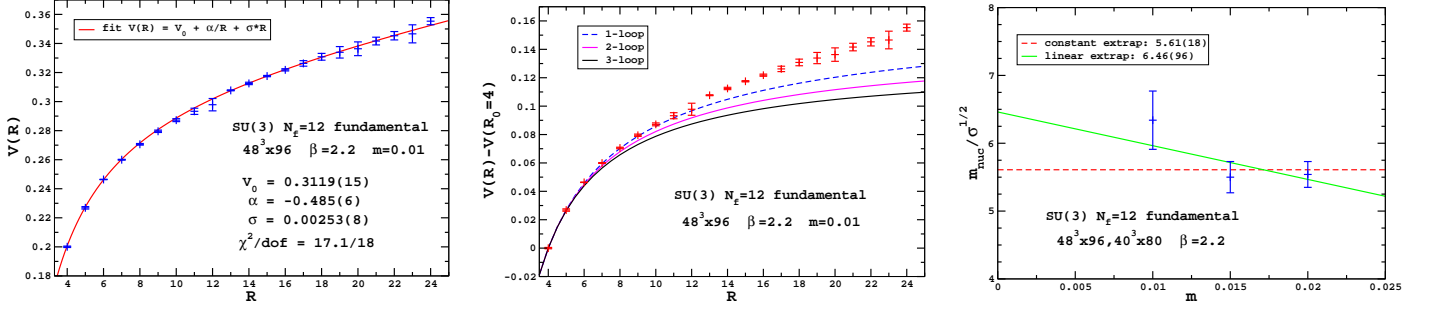


Figure 7:  $V(R)$  data and fit for  $m = 0.01$  is plotted on the left and comparison with perturbation theory is shown in the middle plot. The right side plot shows the string tension measured in nucleon mass units at  $m = 0.01, 0.015, 0.02$  and extrapolated to the chiral limit. The finite nucleon mass gap in the chiral limit implies a finite string tension at  $m = 0$ .

The split remains significant for all fermion masses and in the chiral limit.

#### 2.4. String tension and running coupling from the static force

There are several ways to define a renormalized gauge coupling, for example, the Schrödinger Functional scheme or from square Wilson loops. We take the renormalized coupling as defined via the quark-antiquark potential  $V(R)$ , extracted from  $R \times T$  Wilson loops where the time extent  $T$  can be large. From the potential, one defines the force  $F(R)$  and coupling  $\alpha_{qq}(R)$  as

$$F(R) = \frac{dV}{dR} = C_F \frac{\alpha_{qq}(R)}{R^2}, \quad \alpha_{qq}(R) = \frac{g_{qq}^2(R)}{4\pi}. \quad (5)$$

The coupling is defined at the scale  $R$  of the quark-antiquark separation, in the infinite-volume limit  $L \rightarrow \infty$ . This is different from the scheme using square Wilson loops, where one has  $\alpha_W(R, L)$  and one can choose finite  $R$  with  $L \rightarrow \infty$ , or finite  $L$  and fixed  $R/L$  ratio. In the former case, these schemes are related via

$$\alpha_{qq}(R) = \alpha_W(R)[1 + 0.31551\alpha_W(R) + \mathcal{O}(\alpha_W(R)^2)]. \quad (6)$$

The  $\beta$  function in the qq scheme is known to 3-loops. For SU(3) gauge theory with  $N_f = 12$  fundamental flavors, the location of the infrared fixed point to 3-loop order is  $\alpha_{qq}^* = 0.3714...$  This is about 50% of the scheme-independent 2-loop value of  $\alpha^*$ , indicating that higher order corrections beyond 3-loop might not be negligible.

A range of lattice spacings, volumes and quark masses are studied in the running coupling project, we show results for the largest volume  $48^3 \times 96$  at  $\beta = 2.2$  and quark masses  $m = 0.01$  and  $0.015$  and for the  $40^3 \times 80$  run at  $m = 0.02$ . To improve the

measurement of  $V(R)$ , we use different levels of APE-smearing to produce a correlation matrix of Wilson loops, the lowest energy is extracted using the generalized eigenvalue method. We also improve the lattice force, which is naively discretized as  $F(R + 1/2) = V(R + 1) - V(R)$ . For the Symanzik gauge action, the improvement is a relatively small effect, for example the naive value  $R + 1/2 = 4.5$  is shifted to 4.457866...

In Figure 7 on the left we show the measured  $V(R)$  fitted to the form

$$V(R) = V_0 + \frac{\alpha}{R} + \sigma R. \quad (7)$$

for  $m = 0.01$ . The  $m = 0.015$  and  $m = 0.02$  runs are shown on the right of Figure 7. For all three masses, the resulting fits are good, with a clear signal of linear dependence and an effective string tension  $\sigma$ . The string tension decreases with the quark mass, its behavior in conjunction with the mass spectrum in the chiral limit is under investigation and the first result is shown in the figure. The finite nucleon mass gap in the chiral limit implies a finite string tension at  $m = 0$ .

Table 4:  $m_{\text{nuc}}/\sqrt{\sigma}$ .

$m$	$\sigma$	$\chi^2/\text{dof}$	$m_{\text{nuc}}/\sqrt{\sigma}$
0.01	0.002530(81)	17.1/18	6.34(43)
0.015	0.005147(109)	43.6/17	5.50(23)
0.02	0.007189(77)	6.8/14	5.54(19)

The renormalized coupling  $\alpha_{qq}(R)$  is a derivative of the potential  $V(R)$  and hence more difficult to numerically measure via simulations. The most accurate comparison between lattice simulations and perturbation theory is directly of the potential



$V(R)$  itself. This is naturally given by finite potential differences

$$V(R) - V(R_0) = C_F \int_{R_0}^R \frac{\alpha_{qq}(R')}{R'^2} dR', \quad (8)$$

where  $R_0$  is some reference point where  $\alpha_{qq}(R_0)$  is accurately measured in simulations. From this starting point, the renormalized coupling runs according to perturbation theory, at some loop order. The result is shown in the middle of Figure 7, with curves at 1-, 2- and 3-loop order for the potential difference. Although progress was made in studies of important finite volume effects, more work is needed to bring the systematics under full control. It is worth noting that  $V(R)$  and its slope tend to rise at large  $R$ -values with increasing spatial volumes. In the current state of the analysis the string tension and the fast running coupling are consistent with the  $\chi$ SB hypothesis and do not support the conformal one.

### 2.5. Finite temperature transition

We present some preliminary results from our more extended studies of the finite temperature transition. If the ground state of the model has  $\chi$ SB, a phase transition is expected at some finite temperature in the chiral limit of massless fermions. This phase transition is expected to restore the chiral symmetry. If arguments based on universality, as implemented in a model framework of flavor dependence in the effective  $\Phi^4$ -theory description, were robust as advocated [67], the transition would be found to be of first order. This is not entirely clear and warrants careful continued investigations.

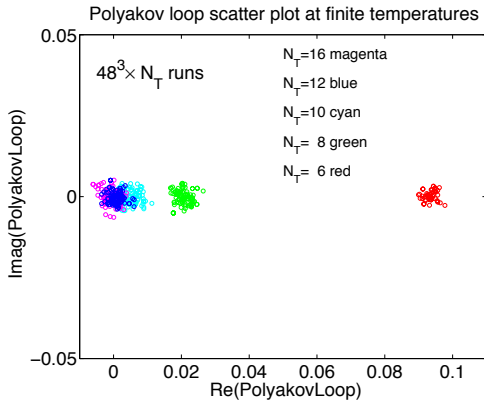


Figure 8: The scatter plot of the Polyakov loop in the time direction as the temperature is varied using lattice sizes in a sequence of lattice sizes  $48^3 \times N_T$  at fixed  $m = 0.01$  with  $N_T$  varied in the  $N_T = 6, 8, 10, 12, 16$  range.

On our largest lattice, at fixed  $m = 0.01$  and  $\beta = 2.2$ , the temperature was varied through an  $N_T$  sequence while the scatter plot of the Polyakov loop was monitored along the euclidean time direction in each run. A clear sudden transition is observed in the  $N_T = 6 - 10$  region where the Polyakov loop distribution jumps from the origin to a scatter plot with non-vanishing real part. It would be more difficult to reconcile this jump, as shown in Figure 8, with conformal behavior in the zero temperature bulk phase.

Although we have results at other gauge couplings, and a variety of fermion masses as the spatial volumes and the temperatures were varied, all consistent with a finite temperature transition, caution is necessary before firm conclusions can be reached. Confirming the existence of the  $\chi$ SB phase transition will require the  $m \rightarrow 0$  limits of  $\langle \bar{\psi}\psi \rangle$  and the Polyakov loop distribution. The chiral condensate is a good order parameter for the transition. The Polyakov loop, like in QCD, could detect deconfinement in the transition with well-known and somewhat problematic interpretation issues.

### 3. Testing the hypothesis of conformal chiral symmetry

The simulation results we presented for twelve fermions in the fundamental representation of the  $SU(3)$  color gauge group favor the chiral symmetry breaking hypothesis. The pion state is consistent with a vanishing mass in the chiral limit and easy to fit with a simple quadratic function of the fermion mass. The non-Goldstone pion spectrum shows very little taste breaking at  $\beta = 2.2$  and the small splittings are consistent with expectations for staggered fermions with stout smearing. The  $SO(4)$  degeneracies and splittings appear to follow the pattern of QCD although the fermion mass dependence is significantly different. The fundamental scale-setting parameter  $F$  of chiral symmetry breaking is finite in the chiral limit.

A non-vanishing chiral condensate is found in the chiral limit which is in the ballpark of the GMOR relation as suggested by the small value of  $F$ . We find a consistent, non-vanishing chiral limit for the subtracted chiral condensate, with the dominant linear UV-contribution removed. The nucleon states, the Higgs ( $f_0$ ) meson, the  $\rho$  meson and  $A_1$  meson extrapolate to non-vanishing masses in the chiral limit and considerable splits of some of the parity partner states persist at very low fermion masses close to the chiral limit. There seems to be an effective string tension indicating confinement-like behavior below the string-breaking scale and the running coupling has not shown signs of a fixed point slowdown. In addition, there seems to be a rapid finite temperature transition whose nature is unclear but hardly favors a conformal bulk phase. Our results are consistent with results reported in [29] but disagree with the chiral analysis of [26] and do not support the infrared fixed point reported in [22].

But is it possible that we mislead ourselves with the  $\chi$ SB interpretation? Can we interpret the results as conformal chiral symmetry? To decide this question, a fairly stringent test is possible. With the conformal hypothesis the mass dependence of all physical states is controlled by the anomalous dimension  $\gamma$  for small fermion masses [35]. Each hadron and  $F_\pi$  should scale as  $M_\pi \approx m^{1/\gamma_m}$  and  $F_\pi \approx m^{1/\gamma_m}$  for small  $m$  where  $\gamma_m = 1 + \gamma$ . For small enough  $m$  the value of  $\gamma$  should be interpreted as  $\gamma^*$  at the infrared fixed point. The chiral condensate is expected to have the behavior  $\langle \bar{\psi}\psi \rangle \approx c \cdot m + m^{\frac{3-\gamma}{1+\gamma}}$  when  $m \rightarrow 0$ . We selected various subsets of states for a combined fit with universal critical exponent  $\gamma$ . We also fitted all measured states combined. Applying the conformal hypothesis to the chiral condensate, to  $F$ , to the pion state, and to the

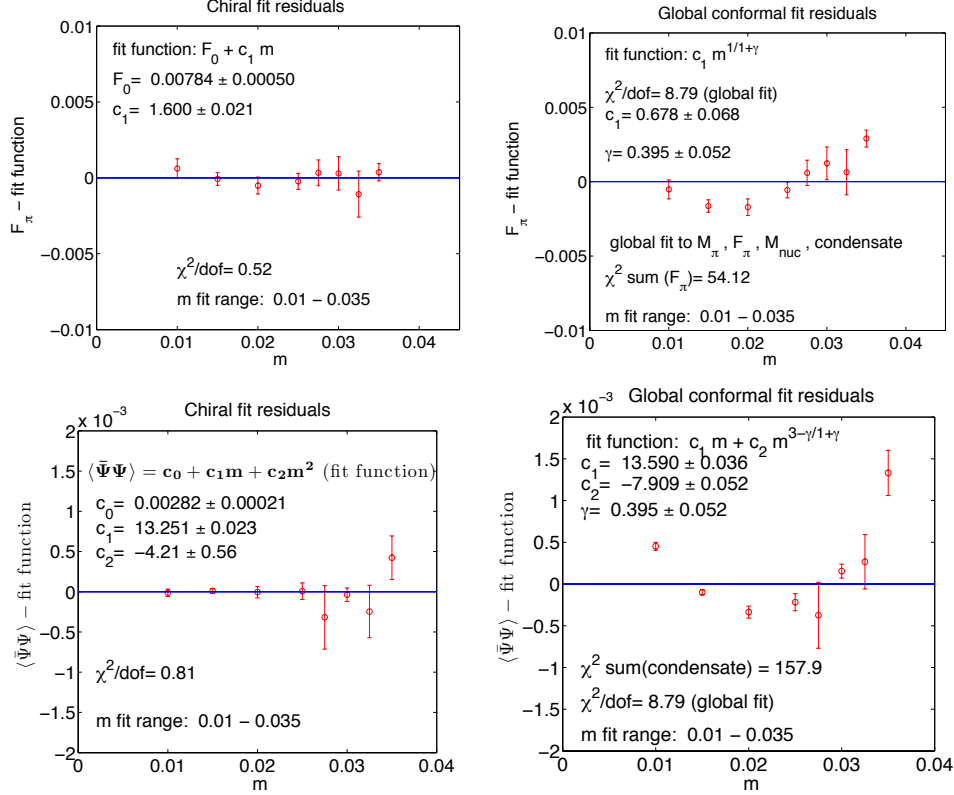


Figure 9: The  $N_f = 12$  chiral and conformal simultaneous fits in four channels are displayed for comparison in two select cases.

stable nucleon state collectively yields a total  $\chi^2 = 229$  for 26 degrees of freedom with  $\chi^2/\text{dof} = 8.79$ . This indicates a very low level of confidence in the hypothesis. The  $\chi\text{SB}$  hypothesis gives  $\chi^2/\text{dof} = 1.22$  for the same set of states. This was the result quoted in Section 1. The chiral and conformal fits for two of the four fitted states with the quoted global results are shown in Figure 9. Applying the global analysis to all states we measured, the contrasting behavior is less pronounced but still significant. The results disfavoring the conformal hypothesis are significant. More work is needed for higher accuracy and full control of the systematics, yet it is worth noting that as the volumes are increased at the lower quark masses, the results for  $F_\pi$  and  $\langle\bar{\psi}\psi\rangle$  will increase or remain the same; this does not bode well for the conformal picture.

#### 4. Conclusions and outlook

We reported new results for a frequently discussed gauge theory with twelve fermion flavors in the fundamental representation of the  $\text{SU}(3)$  color gauge group. Our results favor with a significant level of confidence the  $\chi\text{SB}$  scenario but close to the conformal window several features of this gauge theory clearly differ from QCD. We find a large  $B/F$  ratio which is often interpreted as strong chiral condensate enhancement. This could be related to the fermion mass dependence of the Goldstone pion and the non-Goldstone pion spectra which is different from what is observed in QCD with staggered fermions. In comparison

with QCD, we also observe significantly smaller mass splittings between parity partners in several hadron channels. The near degeneracy of parity partner states is expected to lead to an S-parameter quite different from what was projected when QCD was scaled up by the number of flavors [68]. To gain more confidence in our  $\chi\text{SB}$  analysis, it is important to push deeper into the chiral regime and closer to the continuum limit than the analysis reported earlier [26]. Only future work with high precision simulations will be able to explain whether this is the source of our qualitatively different findings.

The infrared fixed point (IRFP) of the gauge coupling reported earlier [22] is also in disagreement with the picture we presented. It seems to be very difficult to differentiate between an IRFP and a slowly walking gauge coupling close to the conformal window as also indicated with MCRG studies of the model [28]. It would be interesting to establish in a quantitative analysis using the Schrödinger Functional method of [22] and the MCRG method of [28] the difference in the level of confidence between the two mutually exclusive hypotheses of IRFP or walking gauge coupling. This was precisely the main thrust of our work in comparing the  $\chi\text{SB}$  hypothesis with the conformal hypothesis.

We plan the continued investigation of the running gauge coupling reported in Section 2 with the ambitious goal of differentiating between the IRFP and walking gauge coupling scenarios. If a walking gauge coupling  $g_w^2$  can be established approximating IRFP behavior over some extended scale, it will be



important to determine the related mass anomalous dimension  $\gamma(g_w^2)$  and the S-parameter as model examples for BSM applications.

## Acknowledgments

The simulations were performed using computational resources at Fermilab and JLab, under the auspices of USQCD and SciDAC, from the Teragrid structure and at Wuppertal. We are grateful to Kalman Szabo, Sandor Katz, and Stefan Krieg for helping us in using the Wuppertal RHMC code. Simulation on GPU clusters were facilitated by the CUDA ports of [69]. This research is supported by the NSF under grants 0704171 and 0970137, by the DOE under grants DOE-FG03-97ER40546, DOE-FG-02-97ER25308, by the DFG under grant FO 502/1 and by SFB-TR/55, and the EU Framework Programme 7 grant (FP7/2007-2013)/ERC No 208740. D.N. would like to thank the Aspen Center for Physics for invitation to the 2010 BSM summer program. C.R.S. is indebted to the Theory Group at CERN for hospitality at the LGT 2010 workshop.

## References

- [1] S. Weinberg, Phys. Rev. D **19**, 1277 (1979).
- [2] L. Susskind, Phys. Rev. D **20**, 2619 (1979).
- [3] S. Dimopoulos, L. Susskind, Nucl. Phys. **B155**, 237-252 (1979).
- [4] E. Eichten, K. D. Lane, Phys. Lett. **B90**, 125-130 (1980).
- [5] E. Farhi and L. Susskind, Phys. Rept. **74**, 277 (1981).
- [6] B. Holdom, Phys. Lett. **B150**, 301 (1985).
- [7] K. Yamawaki, M. Bando, K. -i. Matumoto, Phys. Rev. Lett. **56**, 1335 (1986).
- [8] T. Appelquist, L. C. R. Wijewardhana, Phys. Rev. **D36**, 568 (1987).
- [9] V. A. Miransky and K. Yamawaki, Phys. Rev. D **55**, 5051 (1997).
- [10] W. E. Caswell, Phys. Rev. Lett. **33**, 244 (1974).
- [11] T. Banks and A. Zaks, Nucl. Phys. B **196**, 189 (1982).
- [12] T. Appelquist, M. Piai, R. Shrock, Phys. Rev. **D69**, 015002 (2004).
- [13] F. Sannino, K. Tuominen, Phys. Rev. **D71**, 051901 (2005).
- [14] D. D. Dietrich, F. Sannino, K. Tuominen, Phys. Rev. **D72**, 055001 (2005).
- [15] M. A. Luty, T. Okui, JHEP **0609**, 070 (2006).
- [16] D. D. Dietrich, F. Sannino, Phys. Rev. **D75**, 085018 (2007).
- [17] M. Kurachi, R. Shrock, JHEP **0612**, 034 (2006). [hep-ph/0605290].
- [18] T. Aaltonen *et al.* [CDF Collaboration], arXiv:1104.0699 [hep-ex].
- [19] E. J. Eichten, K. Lane and A. Martin, arXiv:1104.0976 [hep-ph].
- [20] Z. Fodor, K. Holland, J. Kuti, D. Nogradi and C. Schroeder, Phys. Lett. B **681**, 353 (2009).
- [21] Z. Fodor, K. Holland, J. Kuti, D. Nogradi and C. Schroeder, arXiv:1103.5998 [hep-lat].
- [22] T. Appelquist, G. T. Fleming and E. T. Neil, Phys. Rev. Lett. **100**, 171607 (2008).
- [23] T. Appelquist, G. T. Fleming and E. T. Neil, Phys. Rev. D **79**, 076010 (2009).
- [24] T. Appelquist *et al.*, Phys. Rev. Lett. **104**, 071601 (2010).
- [25] A. Deuzeman, M. P. Lombardo, E. Pallante, Phys. Lett. **B670**, 41-48 (2008).
- [26] A. Deuzeman, M. P. Lombardo, E. Pallante, Phys. Rev. **D82**, 074503 (2010).
- [27] A. Hasenfratz, Phys. Rev. **D80**, 034505 (2009).
- [28] A. Hasenfratz, Phys. Rev. **D82**, 014506 (2010).
- [29] X. -Y. Jin, R. D. Mawhinney, PoS **LAT2009**, 049 (2009).
- [30] X. -Y. Jin, R. D. Mawhinney, PoS **LATTICE2010**, 055 (2010).
- [31] S. Catterall, F. Sannino, Phys. Rev. **D76**, 034504 (2007).
- [32] S. Catterall, J. Giedt, F. Sannino, J. Schneible, JHEP **0811**, 009 (2008).
- [33] A. J. Hietanen, J. Rantaharju, K. Rummukainen, K. Tuominen, JHEP **0905**, 025 (2009).

- [34] A. J. Hietanen, K. Rummukainen, K. Tuominen, Phys. Rev. **D80**, 094504 (2009).
- [35] L. Del Debbio, B. Lucini, A. Patella, C. Pica, A. Rago, Phys. Rev. **D82**, 014510 (2010).
- [36] F. Bursa, L. Del Debbio, L. Keegan, C. Pica, T. Pickup, Phys. Lett. **B696**, 374-379 (2011).
- [37] Y. Shamir, B. Svetitsky, T. DeGrand, Phys. Rev. **D78**, 031502 (2008).
- [38] T. DeGrand, Y. Shamir, B. Svetitsky, Phys. Rev. **D82**, 054503 (2010).
- [39] J. B. Kogut, D. K. Sinclair, Phys. Rev. **D81**, 114507 (2010).
- [40] D. K. Sinclair, J. B. Kogut, PoS **LATTICE2010**, 071 (2010). [arXiv:1008.2468 [hep-lat]].
- [41] E. Bilgici, A. Flachi, E. Itou, M. Kurachi, C. -J. D. Lin, H. Matsufuru, H. Ohki, T. Onogi *et al.*, Phys. Rev. **D80**, 034507 (2009).
- [42] E. Itou, T. Aoyama, M. Kurachi, C. -J. D. Lin, H. Matsufuru, H. Ohki, T. Onogi, E. Shintani *et al.*, PoS **LATTICE2010**, 054 (2010).
- [43] N. Yamada, M. Hayakawa, K. -I. Ishikawa, Y. Osaki, S. Takeda, S. Uno, PoS **LAT2009**, 066 (2009).
- [44] M. Hayakawa, K. -I. Ishikawa, Y. Osaki, S. Takeda, S. Uno, N. Yamada, [arXiv:1011.2577 [hep-lat]].
- [45] R. V. Gavai, Nucl. Phys. **B269**, 530 (1986).
- [46] N. Attig, B. Petersson, M. Wolff, Phys. Lett. **B190**, 143 (1987).
- [47] J. B. Kogut, D. K. Sinclair, Nucl. Phys. **B295**, 465 (1988).
- [48] S. Meyer, B. Pendleton, Phys. Lett. **B241**, 397-402 (1990).
- [49] P. H. Damgaard, U. M. Heller, A. Krasnitz, P. Olesen, Phys. Lett. **B400**, 169-175 (1997).
- [50] S. -y. Kim, S. Ohta, Phys. Rev. **D46**, 3607-3617 (1992).
- [51] F. R. Brown, H. Chen, N. H. Christ, Z. Dong, R. D. Mawhinney, W. Schaffer, A. Vaccarino, Phys. Rev. **D46**, 5655-5670 (1992).
- [52] Y. Iwasaki, K. Kanaya, S. Kaya, S. Sakai, T. Yoshie, Phys. Rev. **D69**, 014507 (2004).
- [53] C. Morningstar and M. J. Peardon, Phys. Rev. D **69**, 054501 (2004).
- [54] Y. Aoki, Z. Fodor, S. D. Katz, K. K. Szabo, JHEP **0601**, 089 (2006).
- [55] C. Urbach, K. Jansen, A. Shindler, U. Wenger, Comput. Phys. Commun. **174**, 87-98 (2006). [hep-lat/0506011].
- [56] T. Takaishi, P. de Forcrand, Phys. Rev. **E73**, 036706 (2006). [hep-lat/0505020].
- [57] S. Durr, Z. Fodor, C. Hoelbling, S. D. Katz, S. Krieg, T. Kurth, L. Lelouch, T. Lippert *et al.*, [arXiv:1011.2711 [hep-lat]].
- [58] J. Gasser and H. Leutwyler, Annals Phys. **158**, 142 (1984).
- [59] H. Leutwyler, Phys. Lett. B **189**, 197 (1987).
- [60] M. Luscher, Commun. Math. Phys. **104**, 177 (1986).
- [61] N. Ishizuka, M. Fukugita, H. Mino, M. Okawa, A. Ukawa, Nucl. Phys. **B411**, 875-902 (1994).
- [62] T. Banks and A. Casher, Nucl. Phys. B **169**, 103 (1980).
- [63] H. Leutwyler, A. V. Smilga, Phys. Rev. **D46**, 5607-5632 (1992).
- [64] J. Bijnens, J. Lu, JHEP **0911**, 116 (2009). [arXiv:0910.5424 [hep-ph]].
- [65] M. Gell-Mann, R. J. Oakes and B. Renner, Phys. Rev. **175**, 2195 (1968).
- [66] R. D. Mawhinney, [hep-lat/9705030].
- [67] R. D. Pisarski, F. Wilczek, Phys. Rev. **D29**, 338-341 (1984).
- [68] M. E. Peskin, T. Takeuchi, Phys. Rev. **D46**, 381-409 (1992).
- [69] G. I. Egri, Z. Fodor, C. Hoelbling, S. D. Katz, D. Nogradi, K. K. Szabo, Comput. Phys. Commun. **177**, 631-639 (2007).